Received: 13 June 2023 | Revised: 5 October 2023 | Accepted: 16 October 2023

DOI: 10.1002/jbm.a.37634

RESEARCH ARTICLE

Society For Biomaterials | WILEY

The influence of pH and salt concentration on the microstructure and mechanical properties of meniscus extracellular matrix-derived implants

Soraya Salinas-Fernandez[1,2,3] | Orquidea Garcia[4] | Daniel J. Kelly[1,2,3,5] | Conor T. Buckley[1,2,3,5]

[1]Trinity Centre for Biomedical Engineering, Trinity Biomedical Sciences Institute, Trinity College Dublin, The University of Dublin, Dublin, Ireland

[2]Discipline of Mechanical, Manufacturing and Biomedical Engineering, School of Engineering, Trinity College Dublin, The University of Dublin, Dublin, Ireland

[3]Advanced Materials and Bioengineering Research (AMBER) Centre, Royal College of Surgeons in Ireland & Trinity College Dublin, The University of Dublin, Dublin, Ireland

[4]Johnson & Johnson 3D Printing Innovation & Customer Solutions, Johnson & Johnson Services, Inc., Irvine, California, USA

[5]Tissue Engineering Research Group, Department of Anatomy and Regenerative Medicine, Royal College of Surgeons in Ireland, Dublin 2, Ireland

Correspondence
Conor T. Buckley, Trinity Centre for Biomedical Engineering, Trinity Biomedical Sciences Institute, Trinity College Dublin, The University of Dublin, Dublin, Ireland.
Email: conor.buckley@tcd.ie

Funding information
Science Foundation Ireland

Abstract

Meniscus-related injuries are a common orthopedic challenge with an increasing incidence in the population. While the preservation of viable meniscal tissue is the preferred approach in repair strategies, complex or total traumatic lesions may require alternative therapeutic approaches such as meniscal reconstruction using allografts or engineered equivalents. Although clinical studies suggest promising outcomes with the use of acellular implants, further development is needed to improve their biological and mechanical requirements. Decellularized extracellular matrix (dECM) derived from menisci is a promising biomaterial for meniscus tissue engineering due to its recapitulation of the native tissue environment and the maintenance of tissue-specific cues. However, the associated mechanical limitations of dECM-derived scaffolds frequently impedes their adoption, requiring additional reinforcement or combining with stiffer biomaterials to increase their load-bearing properties. In this study, decellularized extracellular matrix was extracted and its fibrillation was controlled by adjusting both pH and salt concentrations to fabricate mechanically functional meniscal tissue equivalents. The effect of collagen fibrillation on the mechanical properties of the dECM constructs was assessed, and porcine-derived fibrochondrocytes were used to evaluate in vitro biocompatibility. It was also possible to fabricate meniscus-shaped implants by casting of the dECM and to render the implants suitable for off-the-shelf use by adopting a freeze-drying preservation method. Suture pull-out tests were also performed to assess the feasibility of using existing surgical methods to fix such implants within a damaged meniscus. This study highlights the potential of utilizing ECM-derived materials for meniscal tissue substitutes that closely mimic the mechanical and biological properties of native tissue.

KEYWORDS
biofabrication, ECM, extracellular matrix, meniscus, pH, salt

1 | INTRODUCTION

The incidence of meniscal-related injuries is estimated to be 60 per 100,000 of the population,[1] but their frequency and severity is expected to increase, likely due to greater sport participation in the population and the widespread availability of imaging technology.[2] The prevailing approach for treating meniscus-related lesions is to prioritize the preservation of viable meniscal tissue,[3,4] which provides a better clinical outcome compared to partial or total meniscectomies where the nonviable tissue is removed to avoid knee malfunction and joint degeneration.[5] However, in cases of complex or total traumatic lesions, surgeons rely on alternative therapeutic approaches, in an attempt to re-establish the functionality of the knee joint and mitigate degenerative processes, that would otherwise result from poor knee biomechanics. In those cases, meniscal reconstruction can be performed with the use of either meniscal allograft transplantation or the use of engineered meniscal scaffolds.[6] Commercially and clinically available meniscus implants include the collagen-based CMI® (Stryker Corporation, Kalamazoo, MI, USA),[7,8] the polyurethane based polymeric implant Actifit® (Orteq Ltd., London, UK)[9] and the NUsurface (Active Implants, LLC)[10] manufactured from polycarbonate-urethane (PCU) and reinforced circumferentially with ultra-high-molecular-weight polyethylene (UHMWPE) fibers.[11]

Although various clinical studies highlight promising clinical outcomes from the use of such acellular implants,[8,10] further development is needed to improve their biological and mechanical requirements. Developing biomaterial meniscal equivalents with appropriate biological and mechanical properties could circumvent some of the limitations and concerns associated with the use of allografts, such as donor availability, complex processing requirements, and size-matching issues[12,13] and facilitate improved restoration and integration.[14,15]

Natural menisci possess a complex three-dimensional structure with unique biomechanical properties and biological characteristics. For this reason, identifying an optimal biomaterial for meniscus replacement is crucial for ensuring the long-term success of implants.[16] The use of decellularized extracellular matrix (dECM) has shown promising results for meniscus tissue engineering, preserving the tissue's native environment[17] which provides tissue specific cues for promoting cell proliferation and differentiation.[18,19] Nonetheless, the mechanical limitations of these materials frequently constrain their use, that could potentially result in suboptimal load distribution in the joint or structural fractures of the implanted dECM scaffold leading to a risk of osteoarthritis. By contrast, the native meniscus exhibits a remarkable ability to withstand high mechanical loads and resistance to shear forces, primarily attributed to its unique, tightly packed fiber configuration and distribution.[20,21] Therefore, enhancing the fiber formation of the decellularized extracellular matrix (ECM) could play a pivotal role in augmenting the mechanical properties and functional capacity of meniscal implants.[22]

Several factors have been investigated as methods to control the formation of fibrillar collagen in vitro, such as salt concentration, pH level, temperature and the gelation time.[23–26] Recently, we demonstrated that the mechanical properties of solubilized meniscus dECM-derived constructs could be dramatically improved by modulating the pH and the concentration of the dECM solution, enabling the fabrication of mechanically functional meniscal tissue equivalents.[27] Here we sought to build on this work, by exploring how adjusting the pH and salt concentration in the dECM solution prior to crosslinking regulates collagen fibrillation and hence the mechanical properties of the resulting scaffold (Figure 1). To render scaffolds suitable as off-the-shelf implants, a freeze-drying preservation method was explored and its impact on the microstructure, mechanical performance and suture retention strength of the constructs was evaluated. Finally, in vitro biocompatibility was assessed by culturing porcine-derived fibrochondrocytes. The findings of this work demonstrate the potential for using controlled collagen fibrillation in dECM-derived materials to develop meniscal tissue substitutes with relevant mechanical and biological properties for their implantation as meniscus substitutes.

2 | MATERIALS AND METHODS

2.1 | Decellularization and solubilization of meniscus tissue and hydrogel fabrication

Menisci were harvested from 3-month-old porcine donors. Tissues were minced (1–2 mm) with a scalpel under aseptic conditions and washed with a solution of Dulbecco's phosphate buffered saline (PBS) and 2% penicillin/streptomycin (5000 U/mL, Gibco) for 24 h at −4°C under constant rotation. Next, menisci pieces were freeze-dried using a freeze dryer (FreeZone Triad, Labconco, KC, USA) for 24 h at −10°C and cryomilled (Spex SamplePrep 6770 Freezer/Mill) to obtain a fine powder. For decellularization, cryomilled ECM was immersed in 10 mM Tris–HCl buffer (20 mL of solution per 200 mg of powder) followed by freeze–thaw cycles of freezing at −80°C and heating to 37°C. Three cycles were performed in total, followed by centrifugation at 2500g with the buffer changed for each cycle. After the last cycle, 1% triton-x100 solution (Sigma-Aldrich, Ireland) in PBS was added to the powder and incubated for 24 h under rotation at room temperature (RT). A washing step with ultra-pure water was performed to remove the triton and the tissue was incubated for 24 h at RT in 10 mM Tris–HCl, containing 0.15 M NaCl, 2 mM $MgCl_2$ and 50 U/mL DNase (Sigma-Aldrich, Ireland) with gentle agitation. Two freeze–thaw cycles (from −80°C to 37°C) were performed in 50 mM Tris–HCl buffer with a buffer change after every cycle and a final washing step with ultra-pure water performed.

Decellularized tissue was solubilized in a solution of 0.5 M acetic acid containing 1500 U/mL of pepsin (Sigma-Aldrich, Ireland), under rotation at RT. After 24 h, the solution was centrifuged at 2500g for 1 h and the solubilized supernatant was transferred into a dialysis membrane (MWCO 12–14 kDa, Spectrum™ Labs Spectra/Por™) and dialyzed against deionized water (5 L) for 48 h with three water changes before being freeze-dried. The obtained dry decellularized ECM (dECM) was stored at −80°C until required.

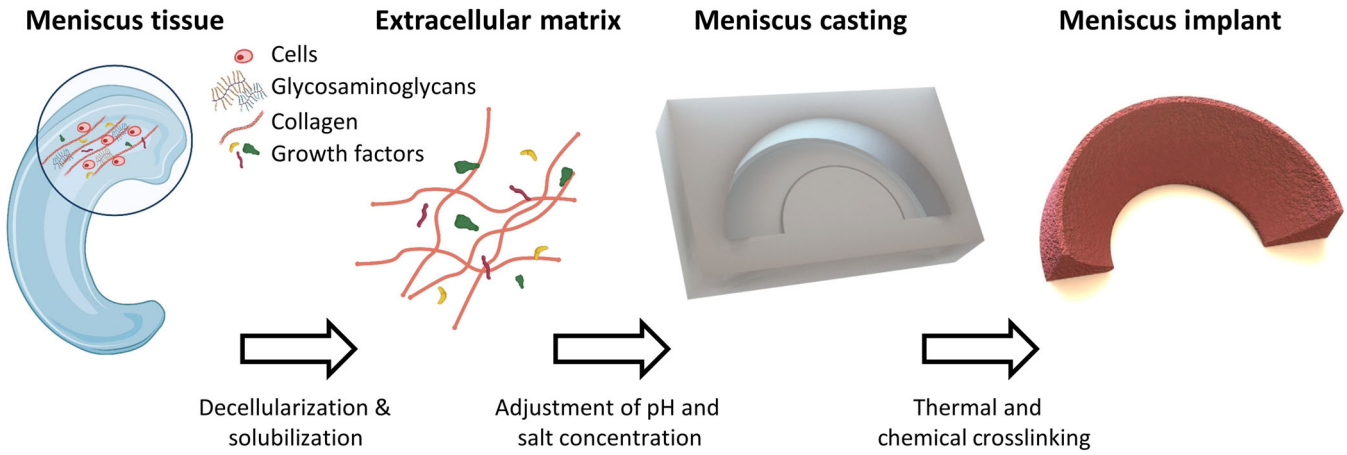

FIGURE 1 Overview of the fabrication process to create decellularized extracellular matrix (dECM) meniscal equivalents. Meniscus tissue was harvested, decellularized, solubilized and pH and salt concentrations were adjusted. Solubilized dECM was cast into a meniscus shaped mold, followed by thermal and chemical crosslinking, to obtain the final meniscus implant. To render implants suitable for off-the-shelf availability, an additional freeze-drying process can be employed.

To create hydrogels, dECM was used at a concentration of 90 or 70 mg/mL. The desired amount of material was weighed and solubilized in 0.5 M of acetic acid containing the appropriate NaCl concentration (0, 50 150, 250 and 300 mM), maintained at 4°C for 48 h. Before use, the pH of the gel was raised to pH 5, pH 7, pH 9 or pH 11, by dropwise addition of a solution of NaOH 10 M, while mixing at 4°C. To ensure proper homogenization of the gel and monitoring of pH changes, phenol red dye was added to the solutions.

2.2 | Characterization of dECM material

Biochemical analyses were performed to quantify sGAG and collagen. Briefly, dECM samples (10 mg) were enzymatically digested in 500 µL of papain (125 µg/mL papain in 0.1 M sodium phosphate with 5 mM Na_2-EDTA and 5 mM cysteine-HCl at pH 6.5) for 18 h at 60°C under rotation. Once digested, sGAG was quantified using a dimethylmethylene blue (DMMB) assay, while the total collagen content was assessed indirectly using a chloramine-T assay, by quantifying the presence of hydroxyproline amino acid within the collagen protein sequence and assuming a hydroxyproline to collagen ratio of 1:7.69.[28] Fourier transform infrared (FT-IR) spectroscopy was used to investigate the degree of collagen denaturation. The transmittance infrared spectrum of dECM, dry meniscus and gelatin Type A were determined from the wavenumber range of 650 to 4000 cm^{-1}, with 64 repeated scans acquired per pixel.

2.3 | Mechanical characterization

Custom-made polydimethylsiloxane (PDMS, SYLGARD™ 184 Silicone Elastomer Kit, Sigma-Aldrich, Ireland) molds were utilized to create cylinders (5 mm × 2 mm) and dog bone specimens for compression and tensile characterization, respectively, from solubilized dECM at the appropriate pH and NaCl concentration. Constructs were incubated at 37°C for 4 h prior to demolding and subsequent crosslinking with 0.5% glutaraldehyde (GA, Sigma-Aldrich, Ireland) in deionized (DI) water with 0, 50, 150, 250 or 300 mM of NaCl at pH 11. After an overnight incubation at RT, the cylinders were rinsed with PBS and washed thoroughly for 4 days.

2.3.1 | Unconfined compression test

Samples were mechanically tested in unconfined compression using a standard materials testing machine with a 10 N load cell (Zwick Z005, Roell, Germany). All tests were performed in a PBS bath at RT. A preload of 0.1*N* was applied to ensure contact with the impermeable loading platens and to ascertain the height of the specimens. Stress-relaxation tests consisted of a ramp and hold cycle with a ramp displacement of 0.02 mm/min until 10% strain was attained and maintained until equilibrium was reached (∼30 min). Dynamic tests were performed immediately after the stress-relaxation cycle whereby the strain was maintained at 10% and a cyclic strain of 1% at 1 Hz was applied for five cycles. Young's modulus was calculated as the slope of the linear region of the stress–strain plot. Within the relaxation phase, the equilibrium modulus was estimated as the equilibrium force divided by the sample's cross-sectional area and the applied strain. Lastly, the dynamic modulus was calculated through the ratio of the determined stress amplitude to the applied strain amplitude.

2.3.2 | Uniaxial tensile test

To determine the tensile properties, dog bone specimens were clamped in custom grips and tested in uniaxial tension. A preload of 0.01*N* was applied before inducing a displacement of 1 mm/min until failure. Elongation at break was determined as the change in length

relative to the original length at which the sample failed, ultimate tensile strength (UTS) was determined as the maximum stress at failure and the tensile modulus was calculated as the slope of the stress–strain plots.

2.4 | Characterization of the microstructure by using scanning electron microscopy

Morphology of dECM samples was assessed by scanning electron microscopy (SEM, Zeiss ULTRA plus). dECM samples were submerged in liquid nitrogen, fractured and freeze dried. Samples were sputter coated with a gold/palladium ratio of 60:40 prior to imaging. High resolution and topographical details of the samples were captured with a Zeiss ULTRA SEM equipment, operating at 5 kV and equipped with a SE2 detector. Images of the microstructure were captured, and pore size was analyzed using Image-J software with magnified regions of SEM images employed to quantitatively assess fiber width.

2.5 | Freeze-drying preservation method

To render the scaffolds suitable for off-the-shelf use a freeze-drying preservation method was employed. Briefly, samples were placed on the cooling shelf of a laboratory grade freeze dryer (FreeZone Triad, Labconco, KC, USA) and cooled to a final freezing temperature (−30°C) using a constant cooling rate (1°C/min) to allow ice crystallization and finally sublimated under vacuum (0.1 mBar) for 18 h at a temperature of −10°C to create the porous network. Constructs subjected to the freeze-drying process were subsequently rehydrated before performing mechanical tests to better represent physiological conditions.

2.6 | Casting of dECM geometrically shaped meniscal implants

An idealized 3D meniscus geometry was created using SOLIDWORKS®. The selected shape and size recreated an average adult native human medial meniscus, consisting of a c-shape of 46 mm length, 24 mm wide and 9.5 mm height.[29] A model was printed using a clear resin and a Formlabs Form 3 stereolithography printer (Formlabs Inc., Somerville, MA, USA). From the positive 3D printed meniscus shape, a negative PDMS mold (SYLGARD™ 184 Silicone Elastomer Kit, Sigma-Aldrich) was formed and thermally cured. For casting, dECM (70 mg/mL) was weighed and solubilized in 0.5 M of acetic acid containing NaCl (150 mM). The solution was rotated at 4°C for 48 h to ensure complete dissolution. Before use, the pH of the slurry was raised to pH 11 by dropwise addition of a solution of NaOH (10 M) at 4°C. Phenol red dye was added to ensure proper homogenization of the gel and monitoring of pH changes. The dECM solution was poured into the negative PDMS mold and subjected to a degassing process by application of a high vacuum for 5 min, with a subsequent incubation for 4 h at 37°C. After demolding, chemical crosslinking was performed using a solution of 0.5% GA in deionized water with a salt concentration of 150 mM and pH 11. After 24 h of incubation at RT, the meniscus shaped implant was rinsed with PBS and washed thoroughly for 4 days.

2.7 | Histological characterization of the dECM geometrically shaped meniscal implants

For histological evaluation, meniscal implants were paraffin wax embedded and sectioned at 7 µm using a microtome (Leica, Germany). Sections were stained with picrosirius red for collagen and immunohistochemistry was performed to detect collagen type I (Abcam, ab138492, 1:400) and collagen type II (Scbt, sc52658, 1:400) as previously described.[30]

2.8 | Evaluation of implant response to suturing

Braided non-absorbable polyester sutures 2-0 (ETIBOND EXCEL®) were used and vertical and horizontal suturing tests were performed. For vertical suturing assessment, perpendicular sutures to the length of the scaffold were placed within the middle of 15 mm wide geometrically shaped meniscal equivalents, 5 mm distance from the outer rim. For the horizontal suturing tests, sutures were placed aligned with the length of the construct, 5 mm from the outer rim. Sutured specimens were mounted in a custom-made device adapted to the mechanical testing machine, where the free ends of the sutures were gripped by the upper tensile clamp, while the samples were situated on the other side of a retaining horizontal plate allowing the application of perpendicular forces to the implant. A pre-load of 0.1*N* was applied to the sutures for 100 s, before applying a load-to-failure test at a rate of 30 mm/min. Load to failure was determined as the first peak defining loss of specimen integrity.

2.9 | In vitro analysis

2.9.1 | Cell isolation and expansion

Under sterile conditions, menisci (medial and lateral) were harvested from 4-month-old porcine donors and rinsed with PBS, containing 100 U/mL penicillin and 100 µg/mL streptomycin. Tissues were minced (1–2 mm) and incubated in pronase (500 U/L) at 37°C for 30 min followed by digestion using a collagenase solution (Collagenase type I, Gibco, 900 U/mL) for 3 h at 37°C under constant agitation. After filtration through a 40 µm cell strainer, the digested material was centrifuged and resuspended in standard culture media (XPAN) consisting of high glucose Dulbecco's modified Eagle's medium (hgDMEM) supplemented with 10% v/v fetal bovine serum (FBS), 100 U/mL penicillin, 100 µg/mL streptomycin and 2.5 µg/mL amphotericin B (all Gibco, Biosciences, Ireland). Separated cells were counted and expanded in monolayer to passage 3.

2.9.2 | Scaffold preparation, cell seeding and viability assessment

dECM cylindrical constructs were formed as described earlier. After rinsing several times with PBS to lower the pH, any remaining GA residues were quenched with glycine 10% and freeze dried as described in Section 2.5. Dried scaffolds were sterilized with 70% ethanol, washed five times with cell media and seeded with fibrochondrocytes at a density of 40,000 cells per construct. Constructs were cultured in XPAN medium at 37°C, and 5% O_2. Cell viability was assessed using the LIVE/DEAD® viability/cytotoxicity assay kit (Invitrogen, Biosciences, Ireland) after 1, 3 and 7 days of cell culture. Briefly, samples were washed with PBS and incubated in a live/dead solution containing 2 μM of calcein AM (live cell membrane, abs/em = 494/517 nm) and 4 μM of ethidium homodimer-1 (dead cell DNA, ex/em = 528/617 nm; both from Cambridge Bioscience, Cambridge, UK) in PBS for 1 h. Samples were then washed in PBS, imaged with a Leica SP8 scanning confocal microscope at 515 and 615 nm channels and assessed using the Leica Application Suite X (LAS X) Software (Version 3.5.5.19976).

2.10 | Statistical analysis

Statistical analysis was performed using GraphPad Prism (version 9). Raw data was tested for normality using a Shapiro–Wilk test and mean and standard deviations were calculated. Assuming a Gaussian distribution, a one-way ANOVA was applied, followed by a Tukey's multiple comparison test between groups. For comparing two groups, unpaired two-tailed Student's *t*-test were performed. Numerical and graphical results are displayed as mean ± SD and significance was accepted at a level of $p < .05$.

3 | RESULTS

3.1 | Decellularization process and characterization of dECM

Native menisci were harvested, minced, washed, dried and further processed to yield a final product termed dECM with a loose fiber network. (Figure 2A). The dry weight collagen content of the final dECM product was 710 ± 20 μg of collagen per mg of dry sample (μg/mg). Furthermore, the GAG content (dry weight) of dECM was 2.2 ± 0.6 μg/mg. An analysis of the secondary structure of the solubilized dECM material by FTIR was performed to assess its possible denaturation and compared to spectra for native meniscus tissue and gelatin type A (Figure 2B). In general, comparable profiles were observed, with the dECM displaying lower transmittances. The absorption band of the dECM included the characteristic peaks of the Amide A (associated with N–H stretching) at 3299 cm^{-1} and Amide B at 2923 cm^{-1}. In the Amide A (i), a much broader spectrum was observed for the gelatin, in comparison to the native meniscus and the dECM. A closer inspection of the Amide I band (ii) showed that the gelatin type A included two distinct peaks at 1632 and 1627 cm^{-1}, whereas the dry meniscus and the solubilized dECM spectra exhibited only one peak each, at 1361 and 1634 cm^{-1} respectively. The calculation of the wavenumber difference ($\Delta\nu$, in cm^{-1}) between the Amide I (ii) and Amide II (iii) (ascribable to N–H stretching mode of the peptide bond) by using the formula $\Delta\nu$ (ν_{ii}-ν_{iii}), was used to assess the maintenance of the triple helical structure within the collagen and is valid for result values <100 cm^{-1},[31] where ν_{ii} is the wavenumber value, in cm^{-1} of the Amide I peak and ν_{iii} is the wavenumber value, in cm^{-1} of the Amide II peak. The triple helical structure was verified for the dry meniscus samples, with a $\Delta\nu$ value of 97 cm^{-1} (where $\nu_{ii} = 1631\ cm^{-1}$, and $\nu_{iii} = 1534\ cm^{-1}$) and the dECM with a $\Delta\nu$ of 86 cm^{-1} (where $\nu_{ii} = 1634\ cm^{-1}$, and $\nu_{iii} = 1548\ cm^{-1}$). However, the gelatin showed a $\Delta\nu$ of 101 cm^{-1} (where $\nu_{ii} = 1632\ cm^{-1}$, and $\nu_{iii} = 1531\ cm^{-1}$) thus indicating the presence of denatured collagen. Finally, the Amide III bands (iv), related to CN stretching and NH and are involved with the triple helical structure of collagen, were characterized by three differentiable peaks, associated with type I collagen. All three peaks were more pronounced for the dECM, at 1282, 1237 and 1203 cm^{-1} (Figure 2B).

3.2 | Enhancing the mechanical performance of the constructs by tuning fibrillation parameters

Solubilized dECM-derived hydrogels formed at pH 5, pH 7 and pH 9 exhibited comparable compressive moduli. In contrast, a significant increase in compressive modulus (sixfold) was observed for constructs formed at pH 11 with increases also observed for the equilibrium (threefold) and dynamic modulus (sixfold increase) relative to constructs formed at pH 5 (Figure 3).

In terms of the effect different concentrations of NaCl salt (0, 50, 150, 250 and 350 mM; Figure 4A), results showed a bell-shaped distribution for all compression tests, where the highest value corresponded to the 150 mM salt concentration for compressive, equilibrium and dynamic modulus. Furthermore, tensile tests were performed on dECM dog bone specimens that were formed using the same pH and salt conditions. No significant differences were observed, with all samples displaying comparable elongation at break values of ~20%, a tensile modulus of ~700 kPa and a dynamic modulus of ~140 kPa (Figure 4B).

To help explain the mechanical testing results, the internal cross-sectional microstructure of constructs formed at pH 11 and different salt concentrations were assessed using SEM (Figure 5). All constructs showed a homogeneously distributed, highly porous network with interconnected pores. The 0 and 350 mM gels exhibited larger pores, whereas the interior of the 150 mM gels contained much smaller pores, although not significantly different from the 50 and 250 mM gels. Pore size was quantified using Image J software, confirming the results observed. Moreover, fiber distribution was assessed, where thicker fibers were observed for 150 mM, that showed significant differences with respect to the thinner fibers measured for the 0 and 350 mM salt concentration.

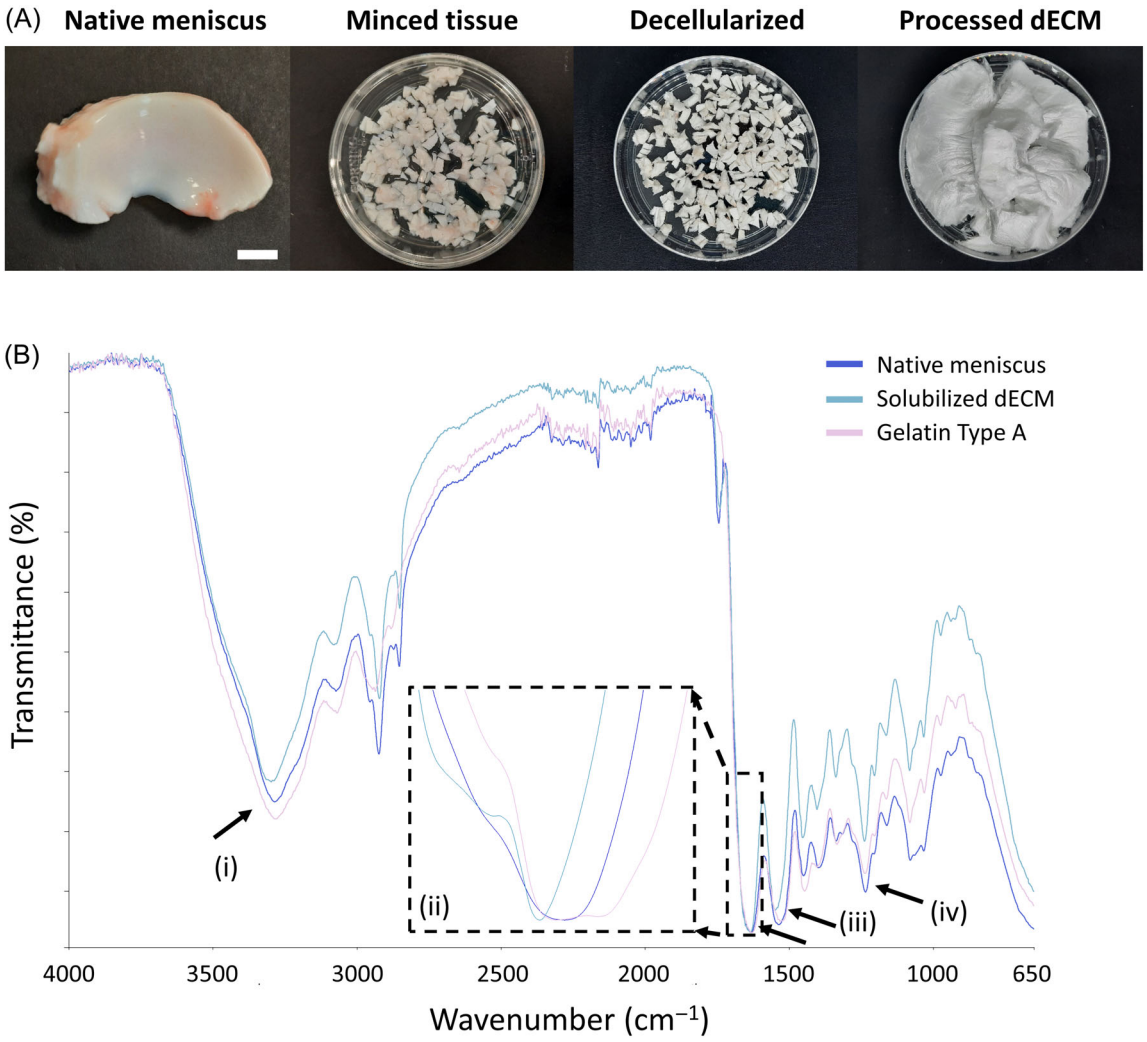

FIGURE 2 (A) Harvested meniscus tissue, and different stages of the solubilization process to produce dECM, scale bar = 10 mm. (B) Comparison of FTIR spectra obtained for dried meniscus tissue, solubilized dECM and gelatin type A. Amide A (i), Amide I (ii), Amide II (iii) and Amide III (iii).

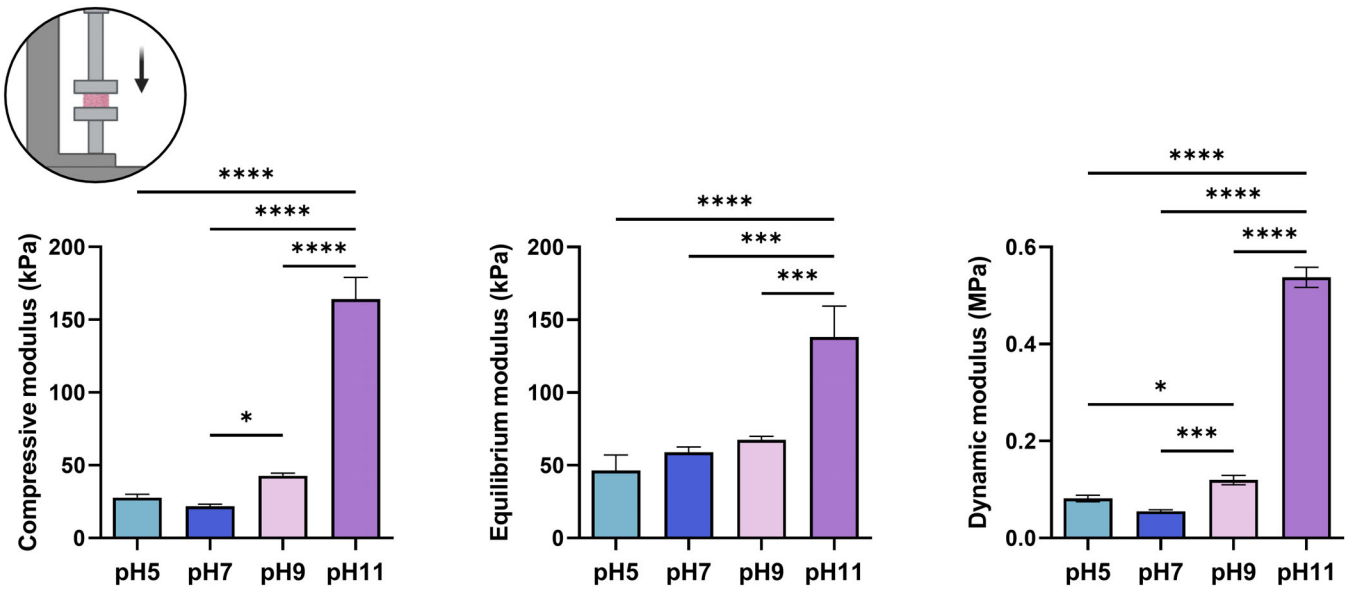

FIGURE 3 Compressive, equilibrium and dynamic moduli of dECM constructs (90 mg/mL), with 150 mM NaCl concentration and different pH levels. Number of replicates, $n = 3$. *, *** and **** indicate significant differences between groups ($p < .05$, $p < .001$ and $p < .0001$, respectively).

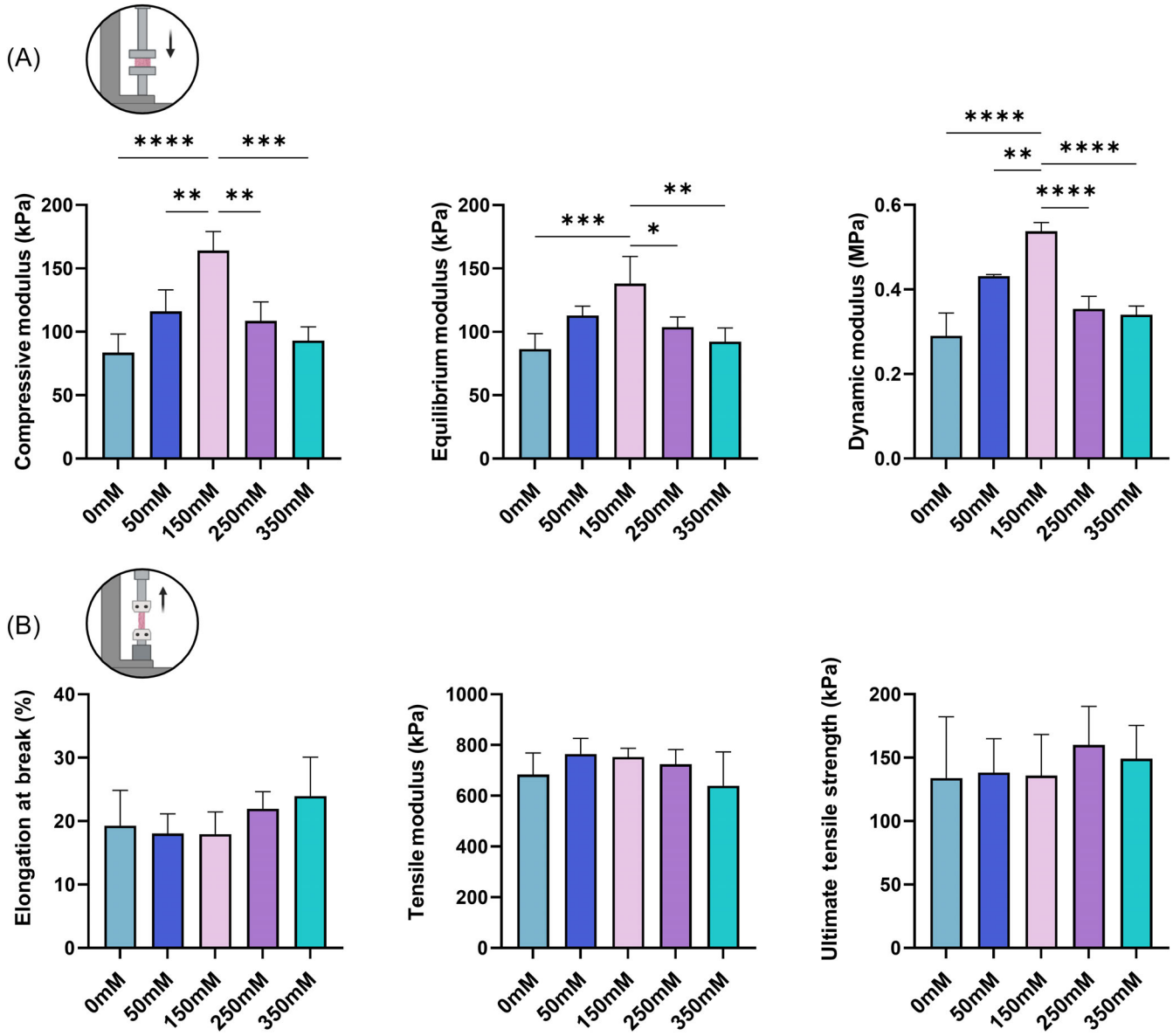

FIGURE 4 Effect of NaCl salt concentration on compressive and tensile properties of dECM constructs (90 mg/mL). (A) Compressive, equilibrium and dynamic moduli of dECM constructs at pH 11 and different NaCl concentrations. (B) Elongation at break, tensile modulus, and ultimate tensile strength of dECM constructs at pH 11 and different NaCl concentrations (0, 50, 150, 250 and 350 mM). Number of replicates, $n = 4$. *, **, *** and **** indicate significant differences between groups ($p < .05$, $p < .01$, $p < .001$ and $p < .0001$, respectively).

3.3 | Influence of freeze-drying on the mechanical properties of dECM constructs

In an attempt to render meniscal constructs suitable for off the shelf availability, a freeze-drying (FD) process was employed (Figure 6A). This was performed for constructs fabricated using two different concentrations of dECM (70 and 90 mg/mL). Preliminary results indicated that 90 mg/mL constructs were prone to fracture when handled, motivating the additional testing of a lower dECM concentration (70 mg/mL) in an attempt to enhance elongation properties. As expected, higher dECM concentrations led to higher compressive mechanical properties (90 mg/mL: 90.6 ± 13.8 kPa; 70 mg/mL: 53.6 ± 7.2 kPa). The FD process had a more pronounced effect at higher concentrations of dECM, but in general reduced the compressive and dynamic properties (but not the equilibrium modulus) compared to the pre-FD controls (Figure 6B). For the pre-FD constructs, both tensile modulus and UTS decreased when lowering the concentration from 90 to 70 mg/mL, with no obvious change in the elongation at break strength (Figure 6C). The FD process also negatively affected both the tensile modulus and UTS, especially for the higher concentration tested. In contrast, the elongation at break strength increased ~2-fold for the 70 mg/mL constructs (Figure 6C).

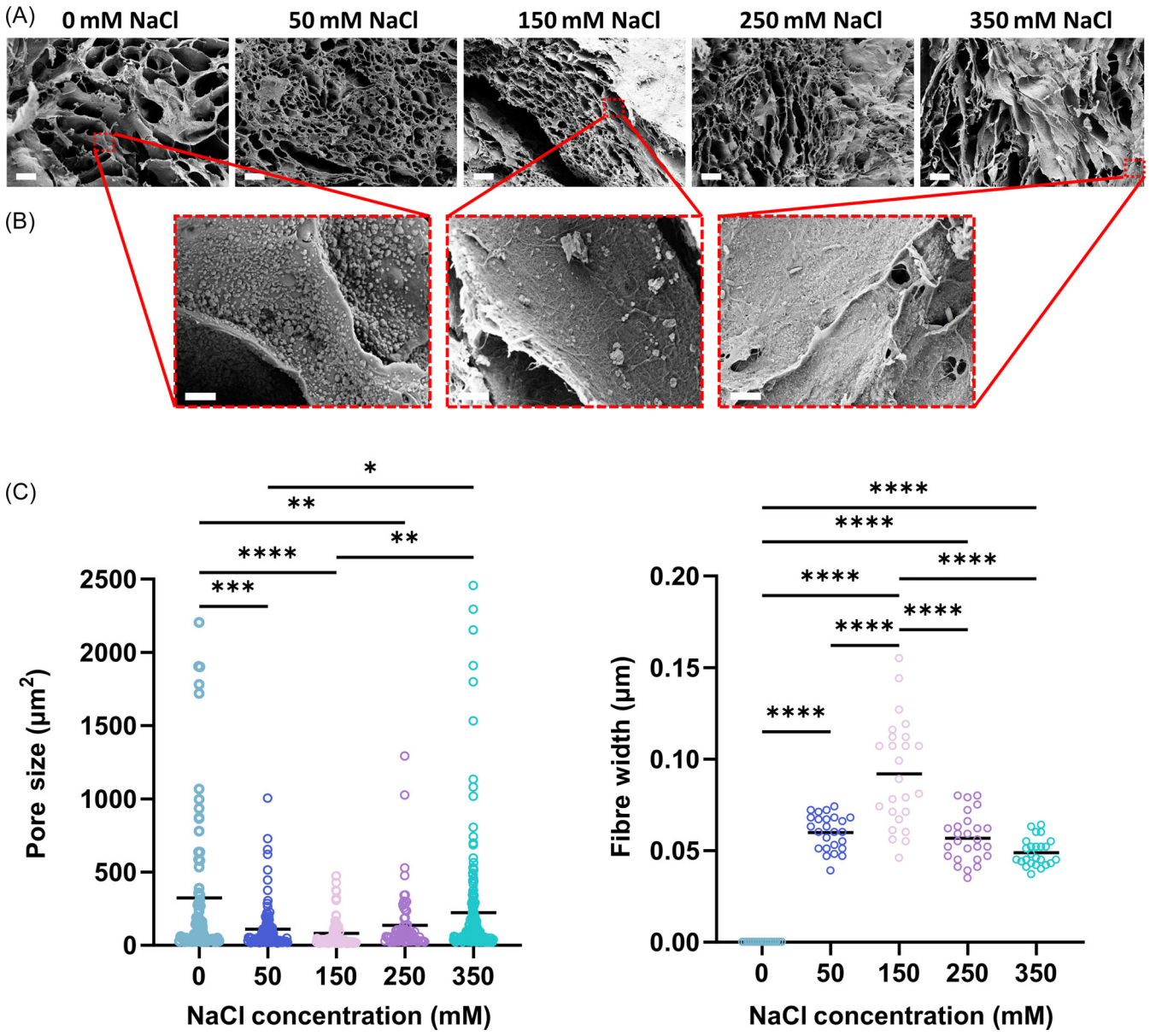

FIGURE 5 (A) SEM images of dECM gels formed with different salt concentrations (scale bar = 40 µm). (B) Higher magnification images of 0, 150 and 350 mM (scale bar = 4 µm). (C) Pore size (μm^2) and fiber width (µm). Number of replicates, $n = 4$. *, **, *** and **** indicate significant differences between groups ($p < .05$, $p < .01$, $p < .001$ and $p < .0001$, respectively).

3.4 | Analysis of an idealized meniscus implant

A full-scale meniscus implant equivalent was cast using a negative PDMS mold. Formed implants maintained their size and shape. Histological analysis revealed a homogeneous distribution of collagen throughout the implant structure (Figure 7A). Post-FD constructs revealed a distinct pore structure, with predominantly elongated pores present. The immunohistochemical staining for collagen type I and collagen type II revealed the uniform presence of both types of collagen within the menisci structures (Figure 7B).

Sutured meniscal implants were assessed using a custom-made device adapted to the mechanical testing machine (Figure 8A). Pre- and post-FD samples were sutured following two different types of suturing regime, vertical (Figure 8B) and horizontal (Figure 8C). Overall, vertical suture strength was higher than horizontal for both pre- and post-FD implants. Pre-FD samples exhibited significantly higher load to failure values for both vertical and horizontal sutures compared to post FD implants (Figure 8C).

3.5 | In vitro biocompatibility of meniscal implants

Freeze-dried meniscus constructs were seeded with fibrochondrocytes and cultured for 7 days. Cells were found to be distributed

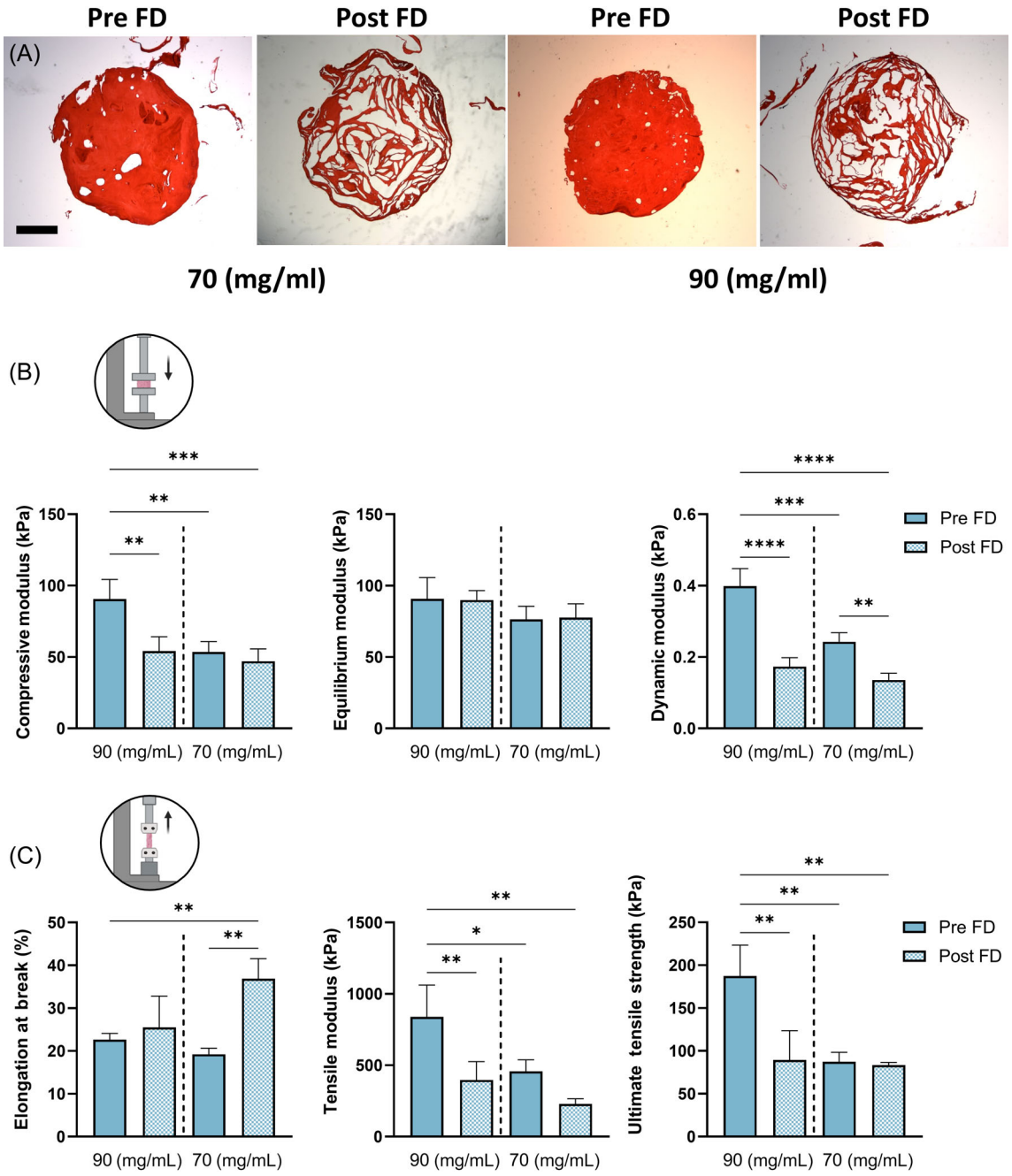

FIGURE 6 Effect of dECM concentration and the freeze-drying process on the internal structure and mechanical performance of dECM constructs, formed at pH 11 and 150 mM NaCl. (A) Constructs stained with picrosirius red before and after the freeze-drying process (Pre FD and Post FD). Scale bar = 1 mm. (B) Compressive, equilibrium and dynamic moduli of dECM constructs formed at 90 and 70 mg/mL pre- and post-freeze drying. (C) Elongation at break, tensile modulus, and ultimate tensile strength of dECM constructs formed at 90 and 70 mg/mL pre- and post-freeze drying. Number of replicates, $n = 4$. *, **, *** and **** indicate significant differences between groups ($p < .05$, $p < .01$, $p < .001$ and $p < .0001$, respectively).

homogenously across the scaffolds, predominantly situated both on the surface within the exterior pores, as observed using confocal microscopy. After day 1 of culture, cells were mostly rounded exhibiting ~75% cell viability. After 3 and 7 days of culture, viability increased to 90% and cells exhibited an elongated morphology (Figure 9).

4 | DISCUSSION

In an attempt to better replicate the native meniscus properties in meniscus replacements, the overall goal of this study was to fabricate an ECM-derived meniscus implant that (i) had appropriate mechanical properties, (ii) could be easily stored for off-the-shelf use to facilitate

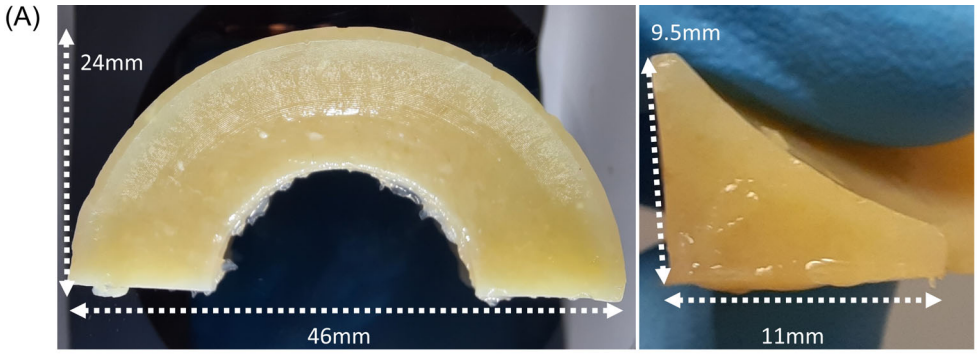

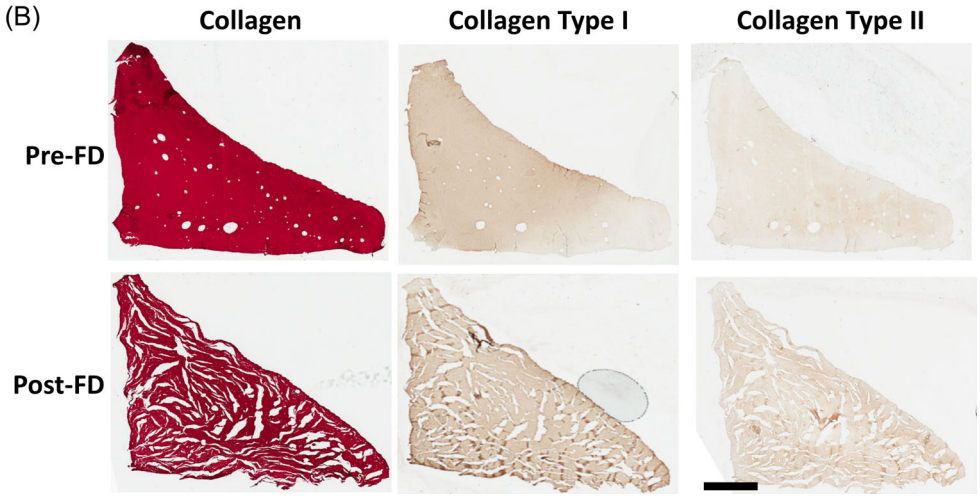

FIGURE 7 Idealized d-ECM meniscus equivalent was fabricated and subjected to a freeze-drying process for off-the-shelf availability. (A) Top and front view of a cast dECM meniscus implant. (B) Sections of the meniscus implant stained with picrosirius red and immunohistochemically stained for collagen types I and II. Scale bar = 2 mm.

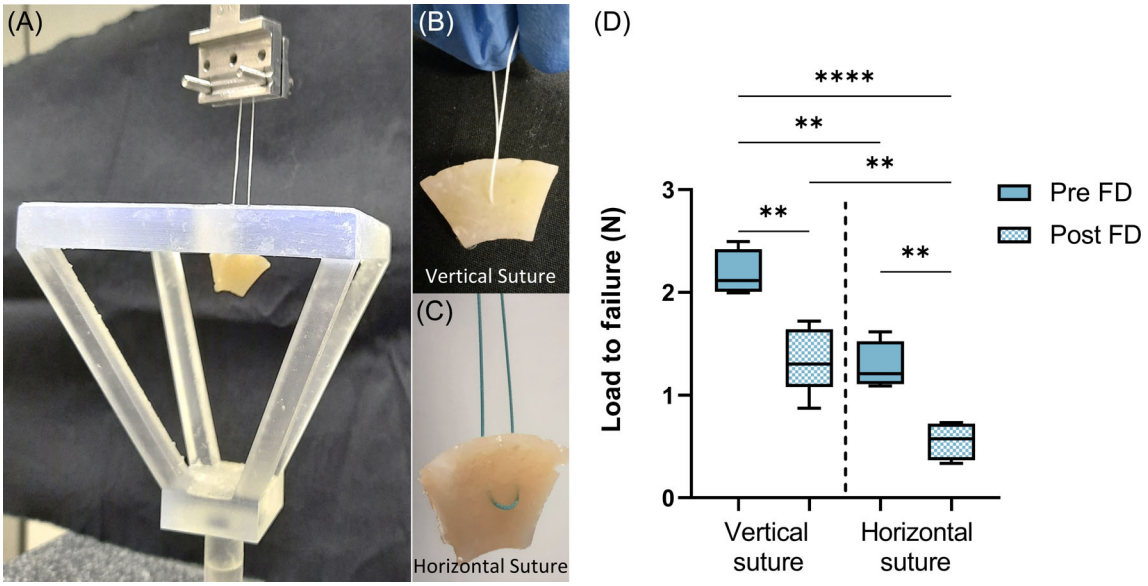

FIGURE 8 Suture pull-out testing. (A) Custom-made device adapted to the mechanical testing machine to assess suture pull out strength. (B) stitched suture in a vertical configuration (vertical suture). (C) Stitched suture in a horizontal configuration (horizontal suture). (D) Maximum load to failure of constructs for vertical and horizontal sutures for both pre- and post-FD implants. Number of replicates, $n = 4$. ** and **** indicate significant differences between groups ($p < .01$ and $p < .0001$, respectively).

manufacturing and clinical translation and (iii) exhibited biocompatibility. To achieve this, porcine meniscus tissue was treated and solubilized using an optimized protocol that avoided collagen denaturation. After the solubilization process, ECM content was found to be

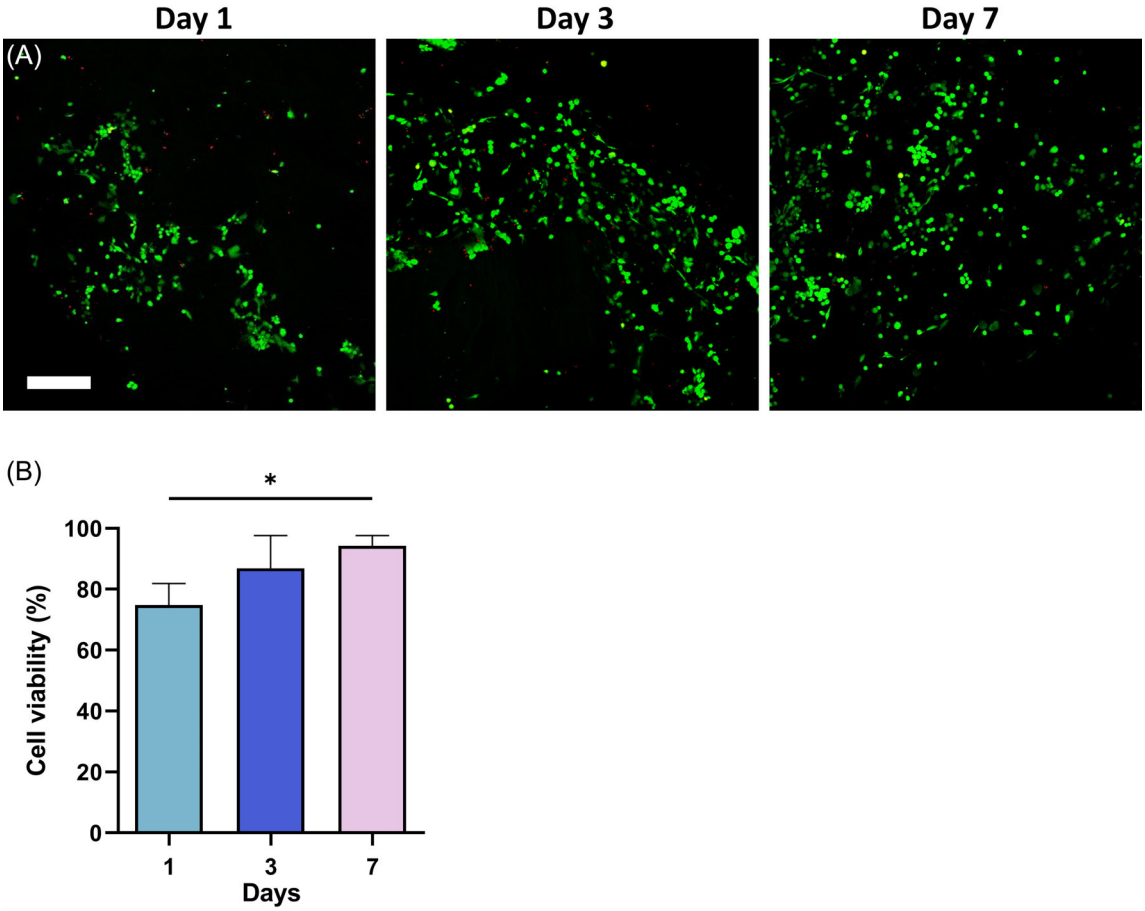

FIGURE 9 (A) Cell viability of fibrochondrocytes seeded on top of freeze-dried meniscus constructs. Live (green) and dead (red) staining of cells after 1, 3 or 7 days of cell seeding. Scale bar = 200 μm. (B) Semi-quantitative analysis of cell viability at 1-, 3- and 7-day post-seeding. Number of replicates, $n = 3$. *Significant differences between groups ($p < .05$).

predominantly collagenous in nature, with a loss in GAG content during the extraction process possibly due to the high solubility of GAGs in water.[32] The use of acidic or alkaline treatments can induce several conformational changes in collagenous materials under thermal exposure,[33] compromising bioactivity and stability.[34] To investigate any potential denaturation of the collagen chains, FTIR analysis was performed on solubilized dECM and compared with the FTIR spectra of dry meniscus and gelatin type A. The dECM spectra were consistent with expected collagen profiles[35] and showed a higher intensity, suggesting a greater collagen concentration in the dECM sample.[36] The observation of the different bands confirmed the maintenance of the triple helical structure in the collagen obtained from the dECM, and the absence of denatured collagen in the extracted material. In fact, in the Amide A, broader peaks have been related to the existence of gelatin in samples extracted at high temperatures,[37] such as the one observed in the FTIR band for gelatin type A (in comparison to the dry meniscus and the extracted dECM profiles). Moreover, the absence of two peaks within the amide I in both dECM and dried meniscus, which are present in the gelatin, verified the stability of the collagen molecular chain within the dECM.[38] Three distinguishable peaks of the Amide III band were present for both dECM and native type I collagen. When examining the spectrum, it is apparent that both dry meniscus and extracted dECM have sharper peaks compared to the less pronounced peaks observed in the gelatin spectra. Typically, wider and less defined peaks at the higher and lower wavelengths indicates that collagen has undergone thermal denaturation.[39] Based on the FTIR results, the decellularization protocol employed successfully preserved the inherent collagen properties in the dECM, which is crucial for maintaining protein fibrillation. Further FTIR assessments on the final casted structures to ensure the non-degradation of collagen on the final dECM implants warrants further investigation.

The next stage entailed regulating the formation of collagen fibers in solubilized meniscus dECM-derived hydrogels. The process of collagen fibrillation depends on electrostatic interactions and alterations to environmental factors such as pH, ionic strength, molecular structure and concentration which can affect the final fiber size, shape and arrangement[40] and ultimately alter the microstructure of collagen gels.[41] Additional crosslinking is normally necessary to enhance the mechanical properties after fibrillogenesis.[42] Therefore, after adjusting the pH of the solution, both thermal and further chemical crosslinking with glutaraldehyde were employed to enhance the mechanical properties. dECM constructs crosslinked at pH 11 exhibited compressive

modulus values comparable to those of native menisci, which have been reported to be in the range of 32.8–137.6 kPa in unconfined compression axial testing, and 40–102 kPa in a radial direction.[43] Constructs exhibited a threefold higher modulus relative to pH 5, pH 7 and pH 9, for the compressive modulus and dynamic modulus, and a twofold increase in the equilibrium modulus, respectively. The large increase of the overall compressive properties at pH 11 can be linked to changes in collagen fibrillation. At a higher pH, the amino acid side chains of collagen become deprotonated, increasing the negative charge of the protein, which enhances the electrostatic interactions. This leads to the formation of thinner and more densely packed fibers[24,44–47] with smaller pore sizes.[48]

The highest menisci implant tensile modulus measured was ~700 kPa. In the native human menisci, however, the tensile modulus ranges from 150 to 200 MPa,[49] which is significantly higher than achieved in this work. Replicating the tensile characteristics of the human meniscus poses a significant challenge primarily due to the unique organization of collagen fibers. Our examination of implants using SEM revealed that the introduction of NaCl had a notable effect on the width of the fibers but did not alter the 3D spatial arrangement of the fibers. As such, different concentrations of NaCl did not appear to affect the tensile properties of these constructs. The highest compressive properties were observed at 150 mM, with the lowest values observed at 0 and 350 mM. These results may be explained by considering the influence of hydrophobic and electrostatic forces on collagen fiber formation. Lower ionic strength has been reported to increase electrostatic and hydrophobic interactions, thereby promoting fibril precipitation and restricting lateral aggregation, resulting in thinner fibrils.[44] In contrast, at 150 mM, electrostatic forces favor the formation of unipolar spindle-shaped D-banded collagen type I fibers, which subsequently merge and mature collectively, leading to the development of wider and structurally organized collagen bundles.[24] In addition to the variation in fiber formation resulting from altered pH and the addition of NaCl, the SEM analysis also suggests that the observed changes in pore size and fiber width can influence mechanical properties. Specifically, at 0 and 350 mM, there was an increase in pore size along with a significant reduction in fiber width, and this combined effect may lead to a decrease in the overall stiffness of the construct.

Following modulation of the construct mechanical properties, we next sought to determine if dry implants more amenable to long-term storage could be produced by freeze-drying of the dECM hydrogels. Meniscal implants have to retain their complex structural physical and biological properties upon implantation, meaning that the preservation method selected for the meniscal implants is key for the desired outcome of the final product.[13,50] For the scope of this project, a freeze-drying process was selected as a preservation method for the dECM meniscal equivalent. Idealized implants were subjected to a freeze drying process to retain their bioactivity and tissue regeneration capacity.[51–53] Moreover, by selecting the freeze-drying parameters, the pore structure can be tailored to impart interconnected pores of desired size and shape.[54,55] The freeze-drying protocol performed in this work introduced large pores, with approximately 50% porosity measured. As expected, introducing changes into the microstructure through freeze drying lowered the compressive and tensile mechanical properties of the final constructs. However, the freeze-drying process did result in enhanced elongation at break properties for the 70 mg/mL constructs. Envisioning the further use of these implants into a clinical environment, where it is important to consider both the mechanical properties and the practical aspects of handling the scaffolds, the 70 mg/mL constructs were selected for further experiments. While the 90 mg/mL scaffolds exhibited superior mechanical properties, they were prone to fracture when handled, which would be unsuitable for clinical use within the knee joint. By reducing the concentration to 70 mg/mL, we observed an improvement in the elongation properties rendering them more suitable for handling. A full-scale idealized meniscal implant was fabricated as a proof of principle. The homogeneous distribution of the collagen differed from the highly organized and compact collagen bundles observed in stained native menisci.[21,56] We observed the presence of both collagen types I and II in our d-ECM meniscus equivalent implants, with stronger staining observed for collagen type I. Precise characterization of the ratio of collagen types I and II using ELISAs may provide deeper insights into how material processing of meniscus tissue affects the final material composition and warrants further investigation. In addition, the suture failure loads observed were much lower in comparison to the high load that native meniscus tissue can support, particularly when using vertical sutures, where strength has been found to reach 200 N.[57,58] For vertical and horizontal sutures in native menisci, the collagen fiber alignment plays an important role in determining the differences in the final load to failure. In the case of the dECM off-the-shelf menisci, the fibers are not highly organized, which perhaps explains the overall decrease in load to failure both in vertical and horizontal sutures. Fabricated implants demonstrated non-cytotoxicity in vitro, promoting cell adhesion and spreading of fibrochondrocytes within the surface pores of the implant. Due to the high density of the material, there were challenges during the cell seeding process with the majority of cells attaching to the surface and external pores of the scaffold, and cell migration was not observed into the interior regions of the implant. However, in an in vivo scenario, where the implant will be subjected to mechanical forces, fluid flow and enzymatic activity influencing material degradation, it is anticipated that the cells could penetrate more readily into the implants over time. Considering the eventual use of these acellular implants, longer experimental time points to gain insights into cell migration and additional in vivo studies could better facilitate the assessment of the tissue–scaffold interactions, in terms of bioactivity and immunogenicity.

5 | CONCLUSION

This work demonstrates that control over the formation of collagen fibers within a dECM matrix can be achieved by adjusting pH and salt concentration to fabricate off-the-shelf mechanically functional meniscal tissue equivalents. By optimizing fibrillation parameters, we

have successfully generated idealized meniscal implants composed entirely of decellularized meniscus extracellular matrix that display promising mechanical properties and biocompatibility. To render implants suitable for long-term storage and hence off-the-shelf availability, a freeze-drying process can be utilized, with the additional benefit of creating a porous structure to facilitate cellular interactions. These findings highlight the potential of utilizing ECM-derived materials for meniscal tissue substitutes that closely mimic the mechanical and biological properties of the native tissue.

ACKNOWLEDGMENTS

This publication was developed with the financial support of Science Foundation Ireland (SFI) under grant numbers 12/RC/2278 and 17/SP/4721. This research was co-funded by the European Regional Development Fund and SFI under Ireland's European Structural and Investment Fund. This research was co-funded by Johnson & Johnson 3D Printing Innovation & Customer Solutions, Johnson & Johnson Services Inc.

CONFLICT OF INTEREST STATEMENT

This research has been co-funded by Johnson & Johnson 3D Printing Innovation & Customer Solutions, Johnson & Johnson Services Inc. An employee of Johnson & Johnson Services Inc. is a co-author of this article.

DATA AVAILABILITY STATEMENT

The data that support the findings of this study are available from the corresponding author upon reasonable request.

ORCID

Conor T. Buckley https://orcid.org/0000-0001-7452-4534

REFERENCES

1. Luvsannyam E, Jain MS, Leitao AR, Maikawa N, Leitao AE. Meniscus tear: pathology, incidence, and management. *Cureus*. 2022;14(5):e25121. doi:10.7759/cureus.25121
2. Bhan K. Meniscal tears: current understanding, diagnosis, and management. *Cureus*. 2020;12(6):e8590. doi:10.7759/cureus.8590
3. Greis PE, Holmstrom MC, Bardana DD, Burks RT. Meniscal injury: II. Management. *J Am Acad Orthop Surg*. 2002;10(3):177-187. doi:10.5435/00124635-200205000-00004
4. Beaufils P, Pujol N. Management of traumatic meniscal tear and degenerative meniscal lesions. Save the meniscus. *Orthop Traumatol Surg Res*. 2017;103(8 Suppl):S237-S244. doi:10.1016/j.otsr.2017.08.003
5. Xu C, Zhao J. A meta-analysis comparing meniscal repair with meniscectomy in the treatment of meniscal tears: the more meniscus, the better outcome? *Knee Surg Sports Traumatol Arthrosc*. 2015;23(1):164-170. doi:10.1007/s00167-013-2528-6
6. Doral MN, Bilge O, Huri G, Turhan E, Verdonk R. Modern treatment of meniscal tears. *EFORT Open Rev*. 2018;3(5):260-268. doi:10.1302/2058-5241.3.170067
7. Buma P, van Tienen T, Veth RP. The collagen meniscus implant. *Expert Rev Med Devices*. 2007;4(4):507-516. doi:10.1586/17434440.4.4.507
8. Lucidi GA, Grassi A, Al-zu'bi BBH, et al. Satisfactory clinical results and low failure rate of medial collagen meniscus implant (CMI) at a minimum 20 years of follow-up. *Knee Surg Sports Traumatol Arthrosc*. 2021;29(12):4270-4277. doi:10.1007/s00167-021-06556-1
9. Leroy A, Beaufils P, Faivre B, Steltzlen C, Boisrenoult P, Pujol N. Actifit® polyurethane meniscal scaffold: MRI and functional outcomes after a minimum follow-up of 5 years. *Orthop Traumatol Surg Res*. 2017;103(4):609-614. doi:10.1016/j.otsr.2017.02.012
10. McKeon BP, Zaslav KR, Alfred RH, et al. Preliminary results from a US clinical trial of a novel synthetic polymer meniscal implant. *Orthop J Sport Med*. 2020;8(9):2325967120952414. doi:10.1177/2325967120952414
11. Elsner J, Condello V, Zorzi C, et al. A novel polycarbonate-urethane meniscal implant: from bench to first clinical experience. *Orthop Proc*. 2012;94-B(Supp_XL):125. doi:10.1302/1358-992X.94BSUPP_XL.ISTA2011-125
12. Cengiz IF, Pereira H, de Girolamo L, et al. Orthopaedic regenerative tissue engineering en route to the holy grail: disequilibrium between the demand and the supply in the operating room. *J Exp Orthop*. 2018;5(1):14. doi:10.1186/s40634-018-0133-9
13. Pereira H, Fatih Cengiz I, Gomes S, et al. Meniscal allograft transplants and new scaffolding techniques. *EFORT Open Rev*. 2019;4(6):279-295. doi:10.1302/2058-5241.4.180103
14. Klarmann GJ, Gaston J, Ho VB. A review of strategies for development of tissue engineered meniscal implants. *Biomater Biosyst*. 2021;4:100026. doi:10.1016/j.bbiosy.2021.100026
15. Mauck RL, Burdick JA. From repair to regeneration: biomaterials to reprogram the meniscus wound microenvironment. *Ann Biomed Eng*. 2015;43(3):529-542. doi:10.1007/s10439-015-1249-z
16. Makris EA, Hadidi P, Athanasiou KA. The knee meniscus: structure-function, pathophysiology, current repair techniques, and prospects for regeneration. *Biomaterials*. 2011;32(30):7411-7431. doi:10.1016/j.biomaterials.2011.06.037
17. Hanai H, Jacob G, Nakagawa S, Tuan RS, Nakamura N, Shimomura K. Potential of soluble decellularized extracellular matrix for musculoskeletal tissue engineering—comparison of various mesenchymal tissues. *Front Cell Dev Biol*. 2020;8:581972. doi:10.3389/fcell.2020.581972
18. Lu H, Hoshiba T, Kawazoe N, Koda I, Song M, Chen G. Cultured cell-derived extracellular matrix scaffolds for tissue engineering. *Biomaterials*. 2011;32(36):9658-9666. doi:10.1016/j.biomaterials.2011.08.091
19. Rothrauff BB, Shimomura K, Gottardi R, Alexander PG, Tuan RS. Anatomical region-dependent enhancement of 3-dimensional chondrogenic differentiation of human mesenchymal stem cells by soluble meniscus extracellular matrix. *Acta Biomater*. 2017;49:140-151. doi:10.1016/j.actbio.2016.11.046
20. Andrews SHJ, Adesida AB, Abusara Z, Shrive NG. Current concepts on structure–function relationships in the menisci. *Connect Tissue Res*. 2017;58(3–4):271-281. doi:10.1080/03008207.2017.1303489
21. Petersen W, Tillmann B. Collagenous fibril texture of the human knee joint menisci. *Anat Embryol (Berl)*. 1998;197:317-324.
22. Kim J, Bonassar LJ. Controlling collagen gelation pH to enhance biochemical, structural, and biomechanical properties of tissue-engineered menisci. *J Biomed Mater Res A*. 2023;111(4):478-487. doi:10.1002/jbm.a.37464
23. Williams BR, Gelman RA, Poppke DC, Piez KA. Collagen fibril formation. Optimal in vitro conditions and preliminary kinetic results. *J Biol Chem*. 1978;253(18):6578-6585.
24. Harris JR, Reiber A. Influence of saline and pH on collagen type I fibrillogenesis in vitro: fibril polymorphism and colloidal gold labelling. *Micron*. 2007;38(5):513-521. doi:10.1016/j.micron.2006.07.026
25. Harris JR, Soliakov A, Lewis RJ. In vitro fibrillogenesis of collagen type I in varying ionic and pH conditions. *Micron*. 2013;49:60-68. doi:10.1016/j.micron.2013.03.004
26. Darvish DM. Collagen fibril formation in vitro: from origin to opportunities. *Mater Today Bio*. 2022;15:100322. doi:10.1016/j.mtbio.2022.100322
27. Wang B, Barceló X, Von Euw S, Kelly DJ. 3D printing of mechanically functional meniscal tissue equivalents using high concentration

extracellular matrix inks. *Mater Today Bio*. 2023;20:100624. doi:10.1016/j.mtbio.2023.100624
28. Ignat'eva NY, Danilov NA, Averkiev SV, Obrezkova MV, Lunin VV, Sobol EN. Determination of hydroxyproline in tissues and the evaluation of the collagen content of the tissues. *J Anal Chem*. 2007;62(1):51-57. doi:10.1134/S106193480701011X
29. Beeler S, Vlachopoulos L, Jud L, et al. Meniscus sizing using three-dimensional models of the ipsilateral tibia plateau based on CT scans – an experimental study of a new sizing approach. *J Exp Orthop*. 2020;7(1):36. doi:10.1186/s40634-020-00252-8
30. Browe DC, Mahon OR, Díaz-Payno PJ, et al. Glyoxal cross-linking of solubilized extracellular matrix to produce highly porous, elastic, and chondro-permissive scaffolds for orthopedic tissue engineering. *J Biomed Mater Res—Part A*. 2019;107(10):2222-2234. doi:10.1002/jbm.a.36731
31. Sizeland KH, Hofman KA, Hallett IC, et al. Nanostructure of electrospun collagen: do electrospun collagen fibers form native structures? *Materialia*. 2018;3:90-96. doi:10.1016/j.mtla.2018.10.001
32. Wu J, Ding Q, Dutta A, et al. An injectable extracellular matrix derived hydrogel for meniscus repair and regeneration. *Acta Biomater*. 2015;16:49-59. doi:10.1016/j.actbio.2015.01.027
33. Zhang X, Xu S, Shen L, Li G. Factors affecting thermal stability of collagen from the aspects of extraction, processing and modification. *J Leather Sci Eng*. 2020;2(1):19. doi:10.1186/s42825-020-00033-0
34. Terzi A, Storelli E, Bettini S, et al. Effects of processing on structural, mechanical and biological properties of collagen-based substrates for regenerative medicine. *Sci Rep*. 2018;8(1):1429. doi:10.1038/s41598-018-19786-0
35. Riaz T, Zeeshan R, Zarif F, et al. FTIR analysis of natural and synthetic collagen. *Appl Spectrosc Rev*. 2018;53(9):703-746. doi:10.1080/05704928.2018.1426595
36. Cebi N, Durak MZ, Toker OS, Sagdic O, Arici M. An evaluation of Fourier transforms infrared spectroscopy method for the classification and discrimination of bovine, porcine and fish gelatins. *Food Chem*. 2016;190:1109-1115. doi:10.1016/j.foodchem.2015.06.065
37. Muyonga JH, Cole CGB, Duodu KG. Fourier transform infrared (FTIR) spectroscopic study of acid soluble collagen and gelatin from skins and bones of young and adult Nile perch (*Lates niloticus*). *Food Chem*. 2004;86(3):325-332. doi:10.1016/j.foodchem.2003.09.038
38. Perez-Puyana V, Ostos FJ, López-Cornejo P, Romero A, Guerrero A. Assessment of the denaturation of collagen protein concentrates using different techniques. *Biol Chem*. 2019;400(12):1583-1591. doi:10.1515/hsz-2019-0206
39. Stani C, Vaccari L, Mitri E, Birarda G. FTIR investigation of the secondary structure of type I collagen: new insight into the amide III band. *Spectrochim Acta Part A Mol Biomol Spectrosc*. 2020;229:118006. doi:10.1016/j.saa.2019.118006
40. Pawelec KM, Best SM, Cameron RE. Collagen: a network for regenerative medicine. *J Mater Chem B*. 2016;4(40):6484-6496. doi:10.1039/c6tb00807k
41. Roeder BA, Kokini K, Sturgis JE, Robinson JP, Voytik-Harbin SL. Tensile mechanical properties of three-dimensional type I collagen extracellular matrices with varied microstructure. *J Biomech Eng*. 2002;124(2):214-222. doi:10.1115/1.1449904
42. Kim YS, Majid M, Melchiorri AJ, Mikos AG. Applications of decellularized extracellular matrix in bone and cartilage tissue engineering. *Bioeng Transl Med*. 2018;4(1):83-95. doi:10.1002/btm2.10110
43. Chia HN, Hull ML. Compressive moduli of the human medial meniscus in the axial and radial directions at equilibrium and at a physiological strain rate. *J Orthop Res*. 2008;26(7):951-956. doi:10.1002/jor.20573
44. Achilli M, Mantovani D. Tailoring mechanical properties of collagen-based scaffolds for vascular tissue engineering: the effects of pH, temperature and ionic strength on gelation. *Polymers (Basel)*. 2010;2(4):664-680. doi:10.3390/polym2040664
45. Christiansen DL, Huang EK, Silver FH. Assembly of type I collagen: fusion of fibril subunits and the influence of fibril diameter on mechanical properties. *Matrix Biol*. 2000;19(5):409-420. doi:10.1016/S0945-053X(00)00089-5
46. Morozova S, Muthukumar M. Electrostatic effects in collagen fibril formation. *J Chem Phys*. 2018;149(16):163333. doi:10.1063/1.5036526
47. Li Y, Asadi A, Monroe MR, Douglas EP. pH effects on collagen fibrillogenesis in vitro: electrostatic interactions and phosphate binding. *Mater Sci Eng C*. 2009;29(5):1643-1649. doi:10.1016/j.msec.2009.01.001
48. Raub CB, Unruh J, Suresh V, et al. Image correlation spectroscopy of multiphoton images correlates with collagen mechanical properties. *Biophys J*. 2008;94(6):2361-2373. doi:10.1529/biophysj.107.120006
49. Fischenich KM, Lewis J, Kindsfater KA, Bailey TS, Haut Donahue TL. Effects of degeneration on the compressive and tensile properties of human meniscus. *J Biomech*. 2015;48(8):1407-1411. doi:10.1016/j.jbiomech.2015.02.042
50. Jacquet C, Erivan R, Sharma A, et al. Preservation methods influence the biomechanical properties of human lateral menisci: an ex vivo comparative study of 3 methods. *Orthop J Sport Med*. 2019;7(4):2325967119841622. doi:10.1177/2325967119841622
51. Joukhdar H, Seifert A, Jüngst T, Groll J, Lord MS, Rnjak-Kovacina J. Ice templating soft matter: fundamental principles and fabrication approaches to tailor pore structure and morphology and their biomedical applications. *Adv Mater*. 2021;33(34):2100091. doi:10.1002/adma.202100091
52. Caliari SR, Harley BAC. The effect of anisotropic collagen-GAG scaffolds and growth factor supplementation on tendon cell recruitment, alignment, and metabolic activity. *Biomaterials*. 2011;32(23):5330-5340. doi:10.1016/j.biomaterials.2011.04.021
53. Browe DC, Díaz-Payno PJ, Freeman FE, et al. Bilayered extracellular matrix derived scaffolds with anisotropic pore architecture guide tissue organization during osteochondral defect repair. *Acta Biomater*. 2022;143:266-281. doi:10.1016/j.actbio.2022.03.009
54. O'Brien FJ, Harley BA, Yannas IV, Gibson L. Influence of freezing rate on pore structure in freeze-dried collagen-GAG scaffolds. *Biomaterials*. 2004;25(6):1077-1086. doi:10.1016/s0142-9612(03)00630-6
55. Grenier J, Duval H, Lv P, et al. Interplay between crosslinking and ice nucleation controls the porous structure of freeze-dried hydrogel scaffolds. *Biomater Adv*. 2022;139:212973. doi:10.1016/j.bioadv.2022.212973
56. Pauli C, Grogan SP, Patil S, et al. Macroscopic and histopathologic analysis of human knee menisci in aging and osteoarthritis. *Osteoarthr Cartil*. 2011;19(9):1132-1141. doi:10.1016/j.joca.2011.05.008
57. Rankin CC, Lintner DM, Noble PC, Paravic V, Greer E. A biomechanical analysis of meniscal repair techniques. *Am J Sports Med*. 2002;30(4):492-497. doi:10.1177/03635465020300040801
58. Stärke C, Kopf S, Petersen W, Becker R. Meniscal repair. *Arthrosc J Arthrosc Relat Surg*. 2009;25(9):1033-1044. doi:10.1016/j.arthro.2008.12.010

How to cite this article: Salinas-Fernandez S, Garcia O, Kelly DJ, Buckley CT. The influence of pH and salt concentration on the microstructure and mechanical properties of meniscus extracellular matrix-derived implants. *J Biomed Mater Res*. 2024;112(3):359-372. doi:10.1002/jbm.a.37634